Check for updates

Chemistry—Methods

Research Article
doi.org/10.1002/cmtd.202500046

Chemistry Europe
European Chemical Societies Publishing

www.chemistrymethods.org

Optimizing Polyoxometalate Electrodes for Energy Storage via Cation Design and Thermal Activation

Lucía Vizcaíno-Anaya, Óscar Giner-Rajala, Carlos Herreros-Lucas, Héctor Rodríguez, and María del Carmen Giménez-López*

Polyoxometalates (POM) are promising materials for electrochemical applications, such as supercapacitors. However, their stability in aqueous electrolytes is compromised due to POM cluster leaching. To mitigate this issue, POM can be combined with organic counter cations, which reduce their solubility in water and influence interactions with carbon support materials. Nevertheless, further research is needed to determine the optimal characteristics and electrode design for maximizing performance. In this work, a synergistic methodology to investigate POM compounds bearing cations with three core functionalities (ammonium, imidazolium, and pyridinium) and varying alkyl side chain lengths, is developed in order to elucidate and optimize the effects of hydrophobicity on the structure of organic–inorganic hybrid materials, electrode films, and their electrochemical performance. The results show that, although cations with long alkyl chains exhibit lower capacitance, they can be activated through molecular rearrangement in the solid state, facilitated by the flexibility of these chains within the structure. By combining thermal and electrochemical techniques, the electrode materials are optimized. These findings demonstrate that the careful selection of counter-cations with the appropriate molecular structures, followed by a thermal activation protocol, is key to developing more efficient and durable energy storage systems.

1. Introduction

Polyoxometalates (POM) are nanometric transition-metal oxide clusters with unique structural features and versatile redox properties,[1] making them highly attractive for electrochemical applications, such as catalysis,[2,3] batteries, and supercapacitors.[4,5] However, POM materials face two major challenges for their implementation in electrodes for energy-related applications. The first challenge is their inherently low electrical conductivity, which has been widely addressed by combining POM with carbon-based support materials.[6–11] The second and more critical challenge is their high solubility in aqueous media due to their anionic nature, leading to the leaching of the POM clusters from the electrode into the electrolyte solution and reducing their stability.[12–14]

One promising approach to addressing this issue involves the incorporation of organic counter cations into the inorganic structure to create hybrid materials with reduced POM solubility. This not only minimizes leaching but also allows for fine-tuning intermolecular interactions with carbon supports,[15] enhancing both stability and electrochemical performance.[16–19] Researchers have explored the use of typical ionic liquid cations as effective modifiers, offering a potential solution to enhance the stability of POM-based electrode materials due to the unique combination of low volatility and high ionic conductivity in ionic liquids.[20–24]

The potential of this approach is exemplified by recent advancements. For instance, aqueous supercapacitors based on $[SiW_{12}O_{40}]^{4-}$ polyoxometalate and imidazolium cations exhibit a stable specific capacitance of 172 F g^{-1} over 1100 cycles.[25] Other works focus on the use of ammonium cations to enhance POM-carbon interactions. In this regard, the group of Gómez–Romero[26] reported the excellent stability up to 10 000 cycles of $[PW_{12}O_{40}]^{3-}$ polyoxometalate with tetraethylammonium cations on activated carbon. Pakulski et al.[27] studied a hybrid material integrating $[Mo_{132}]$ POM anions and dodecyltrimethylammonium cations on graphene, demonstrating prolonged stability over 5000 cycles. More recently, Mu et al.[28] fabricated flexible supercapacitors using polyoxometalate-based materials as efficient electrodes by combining them with cationic amino acids, which enhanced adhesion and electron transfer with various carbon supports.

However, there is still a lack of studies identifying the optimal cation characteristics for maximizing performance, which limits

L. Vizcaíno-Anaya, C. Herreros-Lucas, M. Giménez-López
Centro Singular de Investigación en Química Biolóxica e Materiais Moleculares (CiQUS)
Departamento de Química inorgánica
Universidade de Santiago de Compostela
15782 Santiago de Compostela, Spain
E-mail: maria.gimenez.lopez@usc.es

Ó. Giner-Rajala
Department of Applied Physics
Faculty of Physics and Institute of Materials (iMATUS)
Universidade de Santiago de Compostela
15782 Santiago de Compostela, Spain

H. Rodríguez
CRETUS
Department of Chemical Engineering
Universidade de Santiago de Compostela
15782 Santiago de Compostela, Spain

Supporting information for this article is available on the WWW under https://doi.org/10.1002/cmtd.202500046

© 2025 The Author(s). Chemistry - Methods published by Chemistry Europe and Wiley-VCH GmbH. This is an open access article under the terms of the Creative Commons Attribution License, which permits use, distribution and reproduction in any medium, provided the original work is properly cited.

© 2025 The Author(s). Chemistry - Methods published by Chemistry Europe and Wiley-VCH GmbH

Research Article
doi.org/10.1002/cmtd.202500046
Chemistry Europe
European Chemical Societies Publishing

the optimization of POM-based materials for electrochemical applications. Two key parameters that define a suitable organic cation are the functional group responsible for the positive charge and the surrounding alkyl chains. These structural features influence the hydrophobicity of the resulting compound, directly affecting the stability of the electrode material. However, it should be noted that excessive hydrophobicity can lead to low specific capacitance due to poor wettability and hindered charge transfer.[29,30] This trade-off underscores the importance of carefully selecting molecular structures that balance stability and electrochemical efficiency.

Our study aims to clarify this relationship to facilitate the informed selection of organic counter cations that maintain optimal electrochemical performance in electrode films. To achieve this, we selected the traditional Keggin-type polyoxotungstate of formula $[PW_{12}O_{40}]^{3-}$ (POM) as the active redox anion and combined it with a variety of organic cations commonly used in ionic liquids, featuring different functionalities and alkyl chain lengths: tetrabutylammonium (C4A), dodecyltrimethylammonium (C12A), 1-butyl-3-methylimidazolium (C4Im), 1-dodecyl-3-methylimidazolium (C12Im), 1-butyl-4-methylpyridinium (C4Py), and 1-dodecylpyridinium (C12Py). The hydrophobicity of these cations increases in the order ammonium < imidazolium < pyridinium,[31] and with increasing alkyl chain length,[32] influencing structural assembly and electrochemical properties.

2. Results and Discussion

Scheme 1 represents the structure of all the chosen cations and their abbreviated names based on their main alkyl chain (*i.e.*, C4 or C12) and family (*i.e.*, A, Im, or Py). The compounds were obtained by metathesis in aqueous solution with the expected stoichiometric formula $[cation]_3[PW_{12}O_{40}]$ (see Supporting Information for details), as confirmed by elemental analysis of C, H, and N (Table S1, Supporting Information), indicating no residual precursors are present in the final powders. The samples are labeled as **cation-POM** for short from now on.

After metathesis, the POM structure remains intact, as confirmed by infrared (IR) and Raman spectroscopies (Figure S1 and S2, Supporting Information). The presence of the IR bands located at 1078, 972, and 890 y 810 cm^{-1} correspond to oxygen bonds to: i) a phosphorus atom (P—O_a), ii) a terminal tungsten bond (W—O_d), iii) a bridging bond between tungsten atoms sharing corner (W—O_b—W), and iv) a bridging bond between tungsten atoms sharing edge (W—O_c—W), respectively.[33,34] The most characteristic band of the POM in Raman is located at 1005 cm^{-1} and corresponds to W—O_d bond. Other polyoxometalate bands are located at lower Raman shifts: 995–975 cm^{-1} for W—O_d and P—O_a bonds, 915 cm^{-1} for W—O_b—W bond, 520 cm^{-1} for W—O_c—W bond, and 215 cm^{-1} for W—O_a bond.[35] Organic cations are identified by IR and Raman bands located between 3500 and 1300 cm^{-1}, corresponding to the carbon bonds of the cations.[36] Detailed information can be found in Table S2 and Table S3, Supporting Information.

However, a comparison between the powder X-ray diffraction (PXRD) patterns of the synthesized compounds and the precursor $H_3PW_{12}O_{40}$ (Figure S3, Supporting Information) shows that the organic cations strongly influence their secondary structure. Characteristic peaks at $2\theta = 10.3°$, 25.4°, and 34.6° completely disappear in the new hybrids, while intense peaks at low angles ($2\theta = 2°–9°$) are clearly observed, indicating that the interplanar distance in the structure increases considerably with the incorporation of organic cations (summarized data in Table S4, Supporting Information).[34,37]

Thermal stability of the obtained **cation-POM** hybrid materials was evaluated by thermogravimetric analysis under inert atmosphere (Figure S4, Supporting Information). No weight loss is observed before 400 °C, at which temperature the degradation of the organic cations occurs, with weight losses that agree with the expected $[cation]_3[PW_{12}O_{40}]$ formula (Table S5, Supporting Information). Additionally, a small weight loss (<2 %wt) is observed in all the compounds at temperatures between 550 and 600 °C, corresponding to the decomposition of the POM structure, yielding a final residue composed of a mixture of tungsten and phosphorus oxides.[38]

To assess the role of organic cations in intermolecular interactions, solid–solid and solid–liquid transitions were investigated by differential scanning calorimetry (DSC). It is known that the combination of intermolecular forces within the material (i.e., electrostatic interaction between cations and anions, van der Waals attractions between alkyl chains, and π–π interactions in the presence of aromatic groups) is responsible for the different melting and crystallization temperatures (T_m and T_c, respectively). Moreover, structures with long side chains commonly exhibit solid-phase transitions before melting due to their high flexibility. First, a DSC cycle was performed at lower temperatures to identify solid–solid transitions. As can be observed in Figure S5,

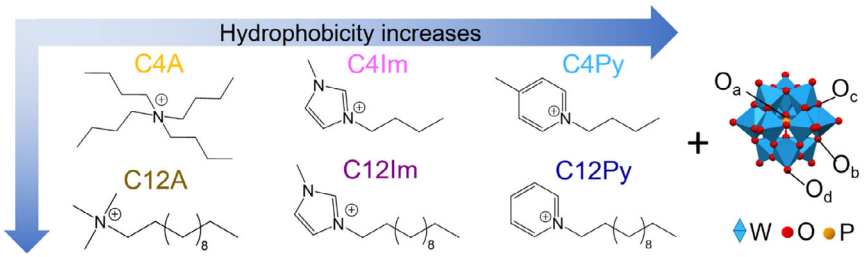

Scheme 1. Molecular structures of the six organic cations that are used to form the cation-POM compounds, indicating the solubility order in water of the different families and alkyl chain lengths, along with polyhedral representation of the Keggin-type POM.

© 2025 The Author(s). Chemistry - Methods published by Chemistry Europe and Wiley-VCH GmbH

26289725, 2025, 9, Downloaded from https://chemistry-europe.onlinelibrary.wiley.com/doi/10.1002/cmtd.202500046 by Uni Santiago Compostela, Wiley Online Library on [27/11/2025]. See the Terms and Conditions (https://onlinelibrary.wiley.com/terms-and-conditions) on Wiley Online Library for rules of use; OA articles are governed by the applicable Creative Commons License

Research Article
doi.org/10.1002/cmtd.202500046
Chemistry Europe
European Chemical Societies Publishing

Supporting Information, compounds with short chains undergo no structural changes in the solid state, in contrast to those with long chains. In particular, **C12Im-POM** (Figure S5d, Supporting Information) and **C12Py-POM** (**Figure 1**a) show a significant endothermic process at 145–155 °C, labeled as "s–h", along with a small exothermic process below 100 °C ("s–c"), which likely corresponds to an incomplete reordering of the chains.[39] In contrast, the sample **C12A-POM** shows several small endothermic peaks up to 213 °C, suggesting that the initial structure is already highly disordered. Additionally, the absence of exothermic processes demonstrates the irreversibility of the structural transition. Transition temperatures and enthalpies are summarized in Table S6, Supporting Information. PXRD analysis of the materials with long cations after this heating–cooling cycle revealed different behaviors. First, the **C12A-POM** result (Figure S6a, Supporting Information) shows the appearance of new intense peaks at low 2θ angles (<5°), which agrees with the irreversibility observed in the DSC curve. Meanwhile, the **C12Im-POM** (Figure S6b, Supporting Information) exhibits almost no change in the XRD pattern, except for a small shift of 0.02° to lower 2θ angles, indicating a highly reversible transition. In contrast, **C12Py-POM** peaks (Figure 1b) present a significant shift of 0.15° to higher 2θ angles, suggesting a decreased separation between chains after solid phase transition. IR and Raman spectra were acquired to confirm that the heating process only affects the secondary structure of the materials and not their molecular integrity (Figure S7, Supporting Information).

To reach the melting transition of the compounds, another DSC experiment was performed in a higher temperature region for two consecutive cycles, with the second one depicted in Figure S8, Supporting Information and Figure 1c. Both T_m and T_c are higher for cations with long alkyl chains due to the increased interaction between chains. However, note that the aromatic ring in **C4Py-POM** sample creates very strong interactions, resulting in high T_m and T_c despite its short alkyl chain, and the highest enthalpies (ΔH_m and ΔH_c) among all samples (Table S7, Supporting Information).

The electrochemical properties of the materials were evaluated on glassy carbon (GC) electrodes in a three-electrode setup using 1 M H_2SO_4 aqueous electrolyte. Nyquist plots (Figure S9a, Supporting Information), obtained by electrochemical impedance spectroscopy (EIS), show a relationship between the charge-transfer resistance (R_{ct}), based on the diameter of the semicircles, and the length of the alkyl chain of the cations. Data were fitted to the standard Randles circuit (Figure S9b, Supporting Information), and the extracted values are summarized in Table S8, Supporting Information. Longer alkyl chains lead to higher R_{ct}, indicating decreased electrode wettability and hindered ionic mobility. In fact, a more pronounced capacitive contribution is observed in the low-frequency region for short-chain cations, as deduced from Bode plots and C′-frequency plots (C′ refers to the real part of the capacitance, obtained from impedance using Equation S(1), Supporting Information) shown in Figure S9c,d, Supporting Information, respectively.[29,40]

Due to the high resistance of the compounds, very low currents are measured in cyclic voltammetry (CV), as observed in Figure S10, Supporting Information. Therefore, mixing them with a conductive support is necessary. For this purpose, carbon black (CB) was added to the inks prior to deposition on the electrodes (further details on electrode preparation are provided in the Experimental section in the Supporting Information). CB is a widely used support material in electrochemistry due to its high

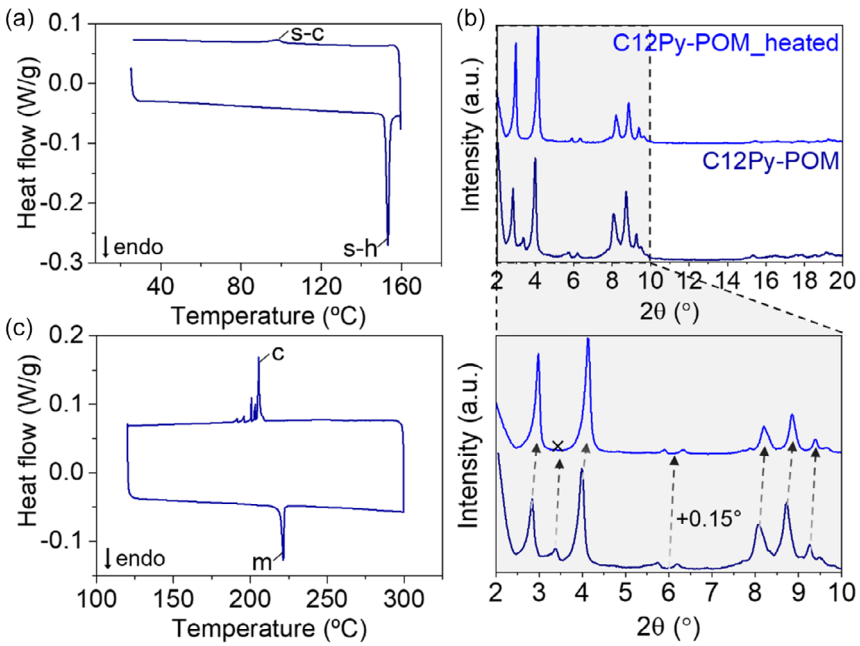

Figure 1. Thermal transitions observed in C12Py-POM as an example of the compounds with long-chain cations. a) DSC curve in the low-temperature region (20–160 °C) showing solid–solid phase transition, indicated as *s–h* in the heating cycle and *s–c* in the cooling cycle. b) PXRD pattern of the material before and after performing DSC up to 160 °C, zooming in the low-angle region where a shift of 0.15° to higher 2θ angles can be observed in the main peaks. c) DSC curve in the high temperature region (120–300 °C) showing melting and crystallization processes indicated as *m* and *c*, respectively.

© 2025 The Author(s). Chemistry - Methods published by Chemistry Europe and Wiley-VCH GmbH

26289725, 2025, 9, Downloaded from https://chemistry-europe.onlinelibrary.wiley.com/doi/10.1002/cmtd.202500046 by Uni Santiago Compostela, Wiley Online Library on [27/11/2025]. See the Terms and Conditions (https://onlinelibrary.wiley.com/terms-and-conditions) on Wiley Online Library for rules of use; OA articles are governed by the applicable Creative Commons License

Research Article
doi.org/10.1002/cmtd.202500046
Chemistry Europe
European Chemical Societies Publishing

surface area, conductivity, chemical stability, and low cost.[41] A POM-to-CB mass ratio of 1:2 was selected, as it provided the highest current density in preliminary CV tests (Figure S11, Supporting Information). **Figure 2**a–c shows an enhanced current and well-defined redox waves, corresponding to the characteristic processes of Keggin POM. These consist of two one-electron transfers and one two-electrons/proton transfer, labeled as I—I′, II—II′, and III—III′, respectively (see Reactions S1–S3, Supporting Information).[42] EIS measurements also confirm a decrease in resistance compared to samples without CB (Figure S12, Supporting Information). The half-wave potentials ($E_{1/2}$) of each redox process in the CV are summarized in Table S9, Supporting Information. As expected, short alkyl-chain cations exhibit more positive $E_{1/2}$ values, as they can stabilize additional negative charges more effectively by surrounding the anion.[43] Among them, **C4Py-POM** shows the most positive $E_{1/2}$ values, likely due to its particularly strong cation interaction in the crystal structure via the aromatic ring, as discussed in DSC measurements. Moreover, current density is significantly higher in samples with short-chain cations compared to long-chain ones, owing to their enhanced wettability. This effect is further demonstrated by measuring the contact angle of a water droplet on the surface of the electrodes. Figure S13, Supporting Information reveals a clear trend in surface wettability: materials containing long alkyl chains exhibit pronounced hydrophobicity, with contact angles of 132°, 145°, and 141° for **C12A-POM**, **C12Im-POM**, and **C12Py-POM**, respectively. In contrast, materials with short-chain cations display highly hydrophilic behavior, with water droplets spreading across the electrode surface (measured contact angles of ≈20°).

A linear relationship between peak currents and scan rate is observed in Figure S14, Supporting Information for all compounds, demonstrating that all redox reactions are surface-confined.[44] Notably, reactions I and II exhibit similar tendencies across all cations, whereas reaction III shows a stronger dependence on scan rate for longer cations compared to shorter ones.

However, a distinct behavior was observed in samples with long chain cations (*i.e.*, **C12A-POM**, **C12Im-POM,** and **C12Py-POM**). Initially, their CV curves displayed very low current densities, which gradually increased with successive cycles, as shown in Figures 2d–f. This suggests that, due to the strong hydrophobicity of the cations, the clusters are initially highly aggregated, limiting the accessible surface area for charge transfer. With continued charge–discharge cycling, the flexible alkyl chains allow for rearrangement in response to anion movement, resulting in an activated material with improved contact between the electrode surface and the electrolyte, thereby increasing the current. The degree of cation hydrophobicity influences the number of cycles required for activation, following the trend: **C12A-POM** (20 scans) < **C12Im-POM** (110 scans) < **C12Py-POM** (600 scans). EIS measurements further confirm this activation, showing a reduced R_{ct}, indicated by a steeper slope in Nyquist plots (Figure S15, Supporting Information). In contrast, shorter cations do not exhibit this rearrangement process due to their limited flexibility and stronger ion-pairing with anions.

Thus, this activation seems to be favored by the presence of long alkyl chains, which were also responsible for solid-phase transitions observed in DSC measurements. To prove that the electrochemical activation is driven by a molecular reordering process similar to that observed in thermal studies, PXRD was performed on the surface of the electrode containing **C12Py-POM** mixed with CB (as a representative long-chain cation material) after CV cycling. As observed in Figure S16, Supporting Information, the material on the electrode shows the same 2θ shift as that observed after heating at 160 °C.

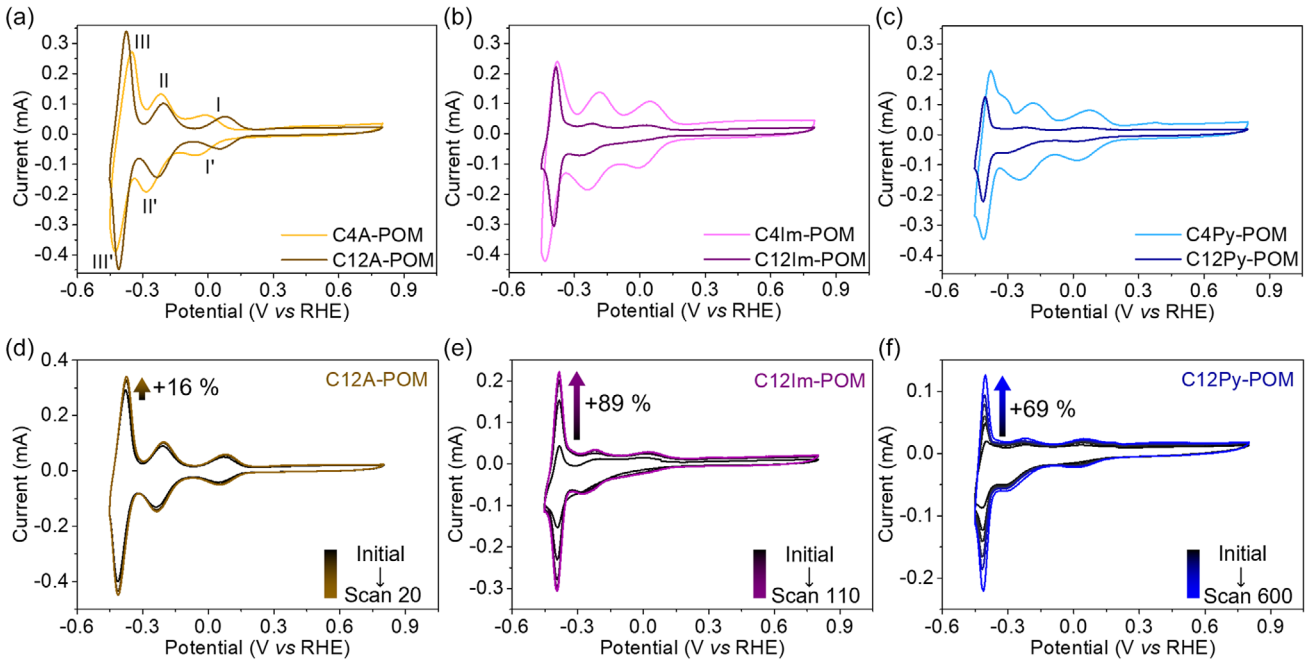

Figure 2. a–c) Cyclic voltammograms of all the compounds, compared by cation family, highlighting the characteristic redox processes. d–f) CV activation of the materials with long alkyl chain cations, showing the number of CV cycles and the percentage increase in the CV areas.

© 2025 The Author(s). Chemistry - Methods published by Chemistry Europe and Wiley-VCH GmbH

26289725, 2025, 9, Downloaded from https://chemistry-europe.onlinelibrary.wiley.com/doi/10.1002/cmtd.202500046 by Uni Santiago Compostela, Wiley Online Library on [27/11/2025]. See the Terms and Conditions (https://onlinelibrary.wiley.com/terms-and-conditions) on Wiley Online Library for rules of use; OA articles are governed by the applicable Creative Commons License

Research Article
doi.org/10.1002/cmtd.202500046
Chemistry Europe
European Chemical Societies Publishing

To further confirm this hypothesis and investigate the distribution of the molecules on the electrode surface, scanning electron microscopy-energy-dispersive X-ray (SEM-EDX) mapping was conducted before and after the activation process for the **C12Py-POM** sample mixed with CB. The results were compared with a sample containing short cations (**C4Py-POM**). At first glance, it is evident that long-chain cations enhance the coverage of the GC electrode surface by CB due to stronger hydrophobic interactions. In contrast, short cations exhibit lower affinity with carbon, resulting in localized material deposition in a single area (Figures S17a,b *vs* Figures S17d,e, Supporting Information). Zoomed-in SEM-EDX mapping of these regions confirms significant POM cluster aggregation in the presence of long cations (Figure S17c, Supporting Information), with particle sizes ranging from 6 to 50 μm, which accounts for the initial low electrochemical response discussed earlier. Conversely, the sample with short cations shows a more homogeneous POM distribution (Figure S17f, Supporting Information).

The electrode with **C12Py-POM** was then subjected to 600 CV activation cycles, after which the surface was analyzed by SEM. Elemental analysis by EDX shows a low weight concentration of W on the surface, likely due to a dilution effect caused by the presence of H_2SO_4 from the electrolyte, as indicated by the high sulphur concentration (≈20 wt%) (Figure S18a, Supporting Information). Nevertheless, tungsten mapping (Figure S18b, Supporting Information) confirms a homogeneous distribution without aggregates, in agreement with the observed electrochemical activation of the material.

To evaluate the stability of all materials, CV cycling was performed for 160 scans. For the long-chain cation samples, cycling was conducted after they had reached their activated state. As can be observed in Figure S19, Supporting Information, the current density of materials with short cations decreases significantly in contrast to those with longer cations. IR spectroscopy was performed on **C4Py-POM** and **C12Py-POM** after CV cycling to verify that the observed decrease in current density is not related to structural degradation of the compounds (Figure S20, Supporting Information). Moreover, the surface of the electrode with **C4Py-POM** was analyzed by SEM (Figure S21a, Supporting Information). In contrast with **C12Py-POM** (Figure S18a, Supporting Information), the concentration of W on the electrode is notably lower (0.1 wt% *vs* 1.3 wt%), which is also evident in the mapping images (Figure S21b, Supporting Information). This confirms that the use of more hydrophilic cations leads to leaching and degradation of the electrode film during charge/discharge cycles due to their weaker interaction with the carbon support and higher affinity for the aqueous electrolyte. **Figure 3** summarizes these findings, illustrating the different CV cycling response

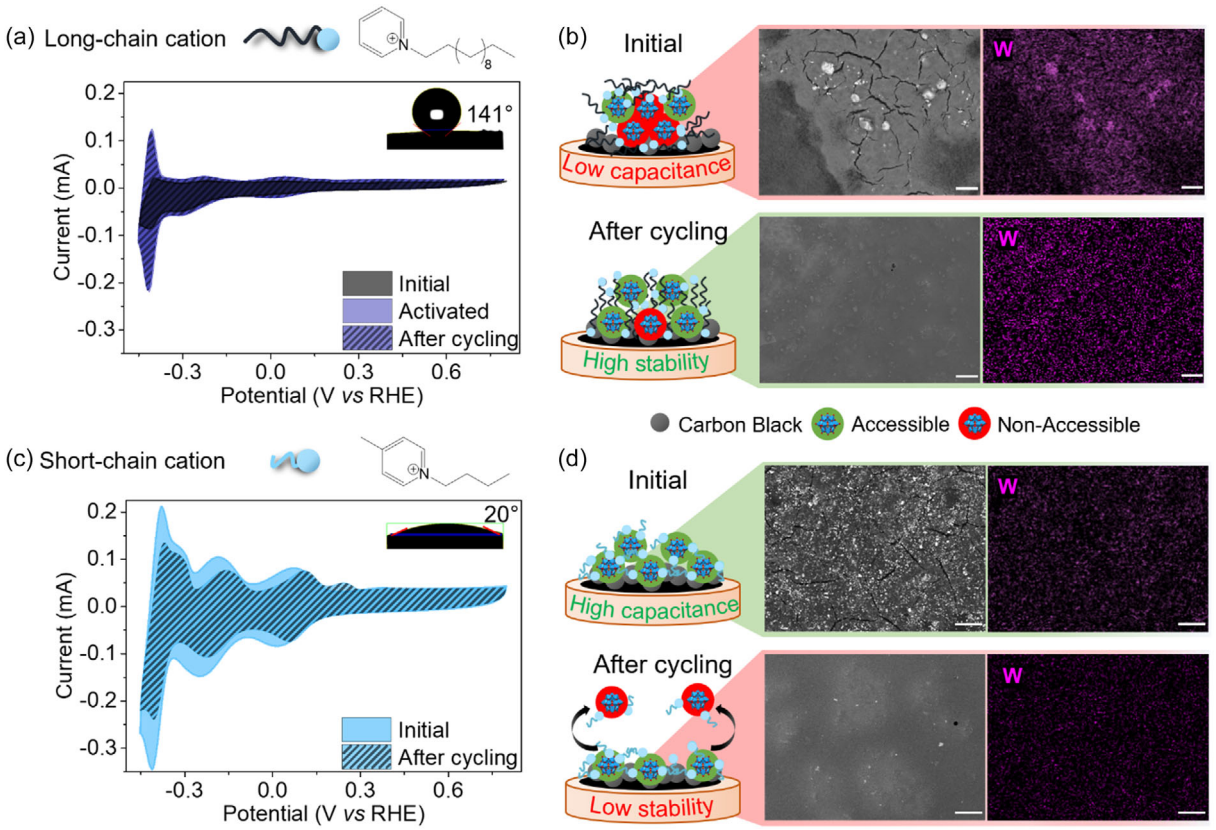

Figure 3. a) Comparison of the initial CV curve of C12Py-POM with the activated curve and the final curve after 160 CV scans. Inset picture corresponds to the contact angle measurement. b) Schematic representation of the activation process occurring in materials with long alkyl chains, including relevant SEM images. Scale bar: 100 μm. c) Comparison of the initial CV curve of C4Py-POM with the final curve after 160 CV scans. Inset picture corresponds to contact angle measurement. d) Schematic representation of the deactivation process of materials with short alkyl chains, including relevant SEM images. Scale bar 100 μm. In the drawings, POM in contact with the aqueous electrolyte, and able to adsorb protons, are labeled as "Accessible". "Non-Accessible" POM refers to POM either covered by the organic layer, which hinders its interaction with protons, or POM no longer in contact with the electrode surface.

© 2025 The Author(s). Chemistry - Methods published by Chemistry Europe and Wiley-VCH GmbH

26289725, 2025, 9, Downloaded from https://chemistry-europe.onlinelibrary.wiley.com/doi/10.1002/cmtd.202500046 by Uni Santiago Compostela, Wiley Online Library on [27/11/2025]. See the Terms and Conditions (https://onlinelibrary.wiley.com/terms-and-conditions) on Wiley Online Library for rules of use; OA articles are governed by the applicable Creative Commons License

Research Article
doi.org/10.1002/cmtd.202500046
Chemistry Europe
European Chemical Societies Publishing

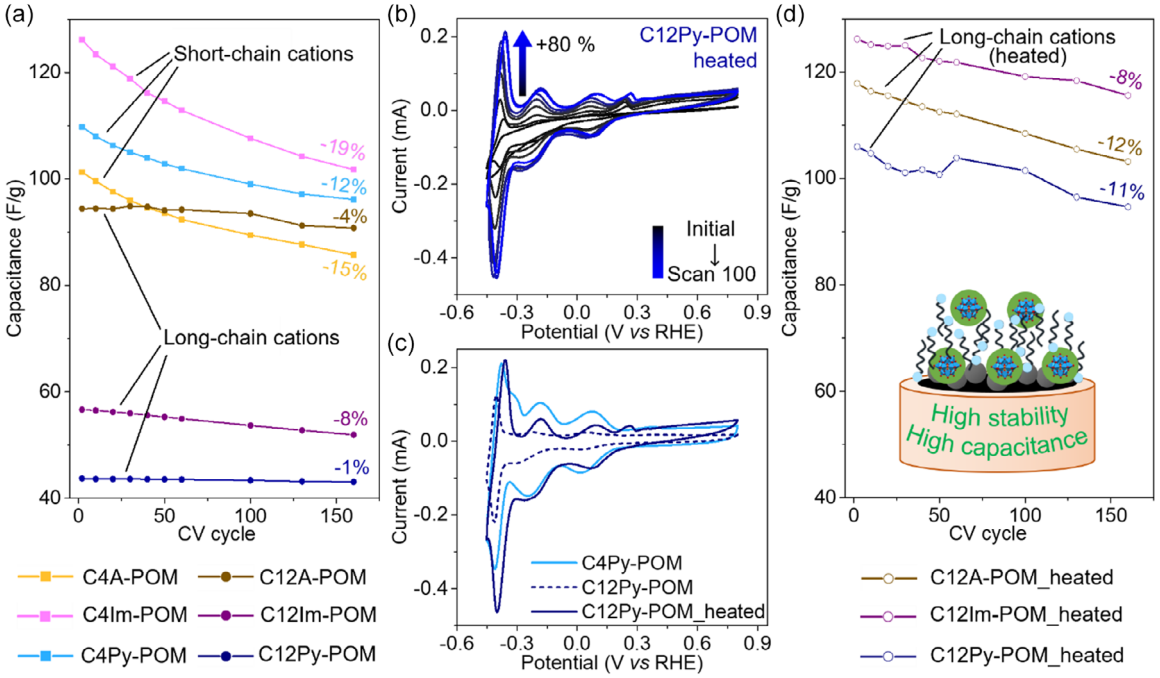

Figure 4. Comparative graphs of the capacitances of the materials with CV cycling. a) Capacitances of all the studied compounds. b) CV activation of thermally treated C12Py-POM, which only requires 100 scans. c) Comparison of CV curves of C4Py-POM, C12Py-POM, and C12Py-POM after thermal and electrochemical activation. d) Capacitances of thermally treated materials with long cations.

of long- and short-chain cations (Figure 3a,c) and providing a schematic representation of the electrode surfaces as inferred from electrochemical and SEM measurements (Figure 3b,d).

The areas within the CV curves at a fixed scan rate of 50 mV s^{-1} were calculated over 160 scans to correlate them with capacitance values and normalized to the mass of cation-POM on the electrodes (20 μg in all cases). As can be observed in **Figure 4**a, samples with short cations such as **C4Im-POM** and **C4Py-POM** exhibit excellent capacitances, with initial values of 126.1 and 109.8 F g^{-1}, respectively, followed by **C4A-POM** with 101.3 F g^{-1}. In contrast, materials with longer alkyl chains display lower capacitance values, which strongly correlate with the hydrophobicity of each cation family, decreasing in the order C12A > C12Im > C12Py. Nevertheless, the stability of the materials follows the opposite trend, as previously discussed with SEM measurements. Highly hydrophobic cations exhibit significantly improved stability (C12Py > C12Im > C12A, all with less than 10% capacitance loss) compared to short-chain cations, which experience capacitance losses of up to 20%.

At this point, the flexibility of the carbon chains has been shown to drive structural rearrangement during both thermal treatment (as evidenced by the solid phase transition in DSC measurements) and electrochemical cycling, leading to an activation of the current response. Based on this, we hypothesized that a similar enhancement in electrochemical performance could be achieved by heating the POM samples prior to preparing the electrodes.

In this experiment, the three POM materials with long cations were first heated at 5 °C min^{-1} to their solid-phase transition temperature (215 °C for **C12A-POM** and 160 °C for the other two). The powders were then mixed with CB, and the electrodes were prepared as before. As shown in Figures S22a–c, Supporting Information and Figure 4b, although the initial CV curves still display low current, activation occurs much more rapidly (e.g., **C12Py-POM** requires only 100 cycles instead of 600), and the final CV areas are significantly larger than those of untreated samples (Figures S22d–f, Supporting Information and Figure 4c). To our knowledge, this type of electrochemical activation has not been previously reported. However, a related study by Otobe et al.[45] described similar conductivity enhancements in crystalline Keggin POM (PW_{12} and SiW_{12}) with dodecylpyridazinium cations (C_{12}Pda), attributed to a solid-state structural transition occurring between 100 and 140 °C.

Finally, these thermally treated samples were further cycled for 160 scans, and the capacitances were calculated as before. Comparing Figure 4a,d, the capacitance increase is substantial, particularly for the more hydrophobic samples (**C12Im-POM** and **C12Py-POM**), which reach initial values comparable to those of the short-chain compounds. Interestingly, although the stability after 160 CV scans is slightly lower than that of the untreated samples, the overall performance is greatly improved, with **C12Im-POM** retaining a capacitance of 115.6 F g^{-1}.

3. Conclusion

In conclusion, our study highlights the crucial role of organic counter cations in optimizing the electrochemical performance of POM-based electrode materials. By using the Keggin-type

© 2025 The Author(s). Chemistry - Methods published by Chemistry Europe and Wiley-VCH GmbH

26289725, 2025, 9, Downloaded from https://chemistry-europe.onlinelibrary.wiley.com/doi/10.1002/cmtd.202500046 by Uni Santiago Compostela, Wiley Online Library on [27/11/2025]. See the Terms and Conditions (https://onlinelibrary.wiley.com/terms-and-conditions) on Wiley Online Library for rules of use; OA articles are governed by the applicable Creative Commons License

$[PW_{12}O_{40}]^{3-}$ polyoxotungstate as the active redox anion and pairing it with organic cations of varying functionalities and alkyl chain lengths, we demonstrated that cation hydrophobicity and flexibility significantly influence the material's structure and electrochemical behavior. DSC results revealed a solid-phase transition around 150 °C in compounds with long alkyl chains, which was attributed to chain rearrangement, as suggested by PXRD analysis. Similar solid–solid transitions have been reported in the literature for materials combining POMs with long-chain organic cations.[46–48] These transitions affect the layer spacing observed in XRD patterns, depending on the nature of the hybrid material. In particular, ionic liquid cations show increasing interplanar distances with rising temperature.[49] In electrochemical tests, long-chain cations initially displayed low current densities, which progressively increased over successive cycles as the materials became activated. This activation, facilitated by the flexible alkyl chains, enhanced electrode–electrolyte contact and reduced charge transfer resistance. Conversely, cations with shorter alkyl chains showed high initial capacitances but lacked the structural flexibility required for further activation. Interestingly, thermal pretreatment of long-chain cation samples accelerated the activation process and enhanced capacitance. Stability tests revealed that more hydrophobic cations exhibited greater durability, with minimal capacitance loss over time. These findings underscore the importance of cation hydrophobicity and flexibility in balancing electrochemical performance and stability, providing a strategy for designing more efficient POM-based electrode materials.

Acknowledgements

This work received financial support from the Ministry of Science of Spain (PID2021-127341OB-I00, TED2021-131451B-C21, and PDC2022-133925-I00 for M.d.C.G.-L.), the European Research Council (ERC) [Starting Grant (NANOCOMP-679124) and ZABCAT (966743) for M.d.C.G.-L.], the Xunta de Galicia (Centro Singular de Investigación de Galicia accreditation 2023–2027, ED431G 2023/03; ED431C 2024/05, the Oportunius Research Professor Program (Gain) for M.d.C.G.-L. and ED431B 2023/22 for H.R.), and the European Union (European Regional Development Fund—ERDF for M.d.C.G.-L.). L.V.-A. acknowledges the Ministry of Universities of Spain for her predoctoral fellowship FPU20/01072.

Conflict of Interest

The authors declare no conflict of interest.

Data Availability Statement

The data that support the findings of this study are available in the supplementary material of this article.

Keywords: capacitance · cations · electrochemistry · electrodes · polyoxometalates

[1] N. I. Gumerova, A. Rompel, *Nat. Rev. Chem.* **2018**, *2*, 0112.
[2] E. P. Quirós-Díez, C. Herreros-Lucas, J. M. Vila-Fungueiriño, L. Vizcaíno-Anaya, Y. Sabater-Algarra, M. del C. Giménez-López, *Small Methods* **2024**, *8*, 2301805.
[3] M. Guillen-Soler, N. V. Vassilyeva, E. P. Quirós-Díez, J. M. Vila-Fungueiriño, A. Forment-Aliaga, M. del C. Gimenez-Lopez, *Adv. Sustainable Syst.* **2024**, *8*, 2300607.
[4] Y. Zhang, J. Liu, S.-L. Li, Z.-M. Su, Y.-Q. Lan, *EnergyChem* **2019**, *1*, 100021.
[5] Y. Zhang, Y. Li, H. Guo, Y. Guo, R. Song, *Mater. Chem. Front.* **2023**, *8*, 732.
[6] Y. Ji, L. Huang, J. Hu, C. Streb, Y. F. Song, *Energy Environ. Sci.* **2015**, *8*, 776.
[7] A. Cao, Y. Li, Z. Chen, Y. Wang, T. Li, Y. Han, *Polymer* **2020**, *204*, 122829.
[8] Z. Chang, X. Sang, Y. Song, X. Sun, X. X. Liu, *Dalton Trans.* **2019**, *48*, 6812.
[9] B. R. Biradar, N. Thathron, P. Pratim Das, S. S. Mal, *J. Electroanal. Chem.* **2024**, *960*, 118192.
[10] H. Dong, J. Cao, Y. Ding, S. Wei, Z. Guo, L. Zhang, X. Zhou, Y. Liao, Q. Zhang, Z. S. Wu, *Chem. Eng. J.* **2024**, *495*, 153509.
[11] J. Gautam, Y. Liu, J. Gu, Z. Ma, B. Dahal, A. Nabi Chishti, L. Ni, G. Diao, Y. Wei, *J. Colloid Interface Sci.* **2022**, *614*, 642.
[12] C. Wang, S. Rong, Y. Zhao, X. Wang, H. Ma, *Transition Met. Chem.* **2021**, *46*, 335.
[13] L. Deng, C. Zhou, Y. Gu, L. Wei, Z. Ma, *Mater. Sci. Eng. B* **2024**, *299*, 117052.
[14] A. Das, M. Mohapatra, S. Basu, *Carbon* **2024**, *223*, 119007.
[15] P. M. Anees, P. R. Chandewar, D. Shee, S. S. Mal, *Energy Technol.* **2024**, *12*, 2400708.
[16] W. Salomon, G. Paille, M. Gomez-Mingot, P. Mialane, J. Marrot, C. Roch-Marchal, G. Nocton, C. Mellot-Draznieks, M. Fontecave, A. Dolbecq, *Cryst. Growth Des.* **2017**, *17*, 1600.
[17] X. Wu, W. Wu, Q. Wu, W. Yan, *Langmuir* **2017**, *33*, 4242.
[18] C. Huez, S. Renaudineau, F. Volatron, A. Proust, D. Vuillaume, *Nanoscale* **2023**, *15*, 10634.
[19] M. Razlansari, M. Kahrizi, A. Rahdar, A. M. Díez-Pascual, *Inorg. Chem. Commun.* **2024**, *159*, 111820.
[20] A. Misra, K. Kozma, C. Streb, M. Nyman, *Angew. Chem., Int. Ed.* **2020**, *59*, 596.
[21] S. Herrmann, A. Seliverstov, C. Streb, *J. Mol. Eng. Mater.* **2014**, *2*, 1440001.
[22] J. Miao, M. Huang, W. Sun, Z. Weng, Q. Wu, T. Gui, Q. Xu, X. Li, H. Pang, *J. Colloid. Interface Sci.* **2025**, *688*, 562.
[23] Y. Zhou, J. Sun, S. Gallet, J. Raya, C. Boudon, A. Bonnefont, L. Ruhlmann, V. Badets, *ChemCatChem* **2024**, *16*, e202400226.
[24] D. Cheng, Z. Gao, W. Wang, S. Li, B. Li, H.-Y. Zang, *Polyoxometalates* **2023**, *2*, 9140019.
[25] M. Ammam, J. Fransaer, *J. Electrochem. Soc.* **2011**, *158*, A14.
[26] J. J. Zhu, R. Benages-Vilau, P. Gomez-Romero, *Electrochim. Acta* **2020**, *362*, 137007.
[27] D. Pakulski, A. Gorczyński, W. Czepa, Z. Liu, L. Ortolani, V. Morandi, V. Patroniak, A. Ciesielski, P. Samorì, *Energy Storage Mater.* **2019**, *17*, 186.
[28] C. Mu, Z. Du, W. Li, *Polyoxometalates* **2024**, *3*, 9140062.
[29] B. Fang, L. Binder, *J. Phys. Chem. B* **2006**, *110*, 7877.
[30] K. Dujearic-Stephane, M. Gupta, A. Kumar, V. Sharma, S. Pandit, P. Bocchetta, Y. Kumar, *J. Compos. Sci.* **2021**, *5*, 66.
[31] E. Can, A. Jalal, I. G. Zirhlioglu, A. Uzun, R. Yildirim, *J. Mol. Liq.* **2021**, *332*, 115848.
[32] Y. Cao, Y. Chen, X. Sun, Z. Zhang, T. Mu, *Phys. Chem. Chem. Phys.* **2012**, *14*, 12252.
[33] T. Okuhara, N. Mizuno, M. Misono, in *Advances in Catalysis*, Academic Press **1996**, *41*, pp. 113–252.
[34] T. Rajkumar, G. Ranga Rao, *J. Chem. Sci.* **2008**, *120*, 587.
[35] Ž. Mravik, D. Bajuk-Bogdanović, A. Mraković, L. Vukosavljević, I. Trajić, J. Kovač, D. Peruško, N. Gavrilov, Z. Jovanović, *Radiat. Phys. Chem.* **2021**, *183*, 109422.
[36] Z. E. A. Abdalla, B. Li, A. Tufail, *Colloids Surf., A* **2009**, *341*, 86.
[37] C.-B. Hong, T. Wang, H. Liu, *Inorg. Chem.* **2023**, *62*, 4054.
[38] S. R. Mane, R. M. Mane, P. S. Patil, P. N. Bhosale, *Adv. Mater. Lett.* **2013**, *4*, 94.
[39] M. Nyman, D. Ingersoll, S. Singh, F. Bonhomme, T. M. Alam, C. J. Banker, M. A. Rodriguez, *Chem. Mater.* **2005**, *17*, 2885.
[40] D. Kumar, A. K. Tomar, S. Singal, G. Singh, R. K. Sharma, *J. Power Sources* **2020**, *462*, 228173.
[41] N. S. Mughal, D. A. Walsh, G. N. Newton, *ACS Appl. Energy Mater.* **2020**, *3*, 12308.
[42] M. Sadakane, E. Steckhan, *Chem. Rev.* **1998**, *98*, 219.

© 2025 The Author(s). Chemistry - Methods published by Chemistry Europe and Wiley-VCH GmbH

26289725, 2025, 9, Downloaded from https://chemistry-europe.onlinelibrary.wiley.com/doi/10.1002/cmtd.202500046 by Uni Santiago Compostela, Wiley Online Library on [27/11/2025]. See the Terms and Conditions (https://onlinelibrary.wiley.com/terms-and-conditions) on Wiley Online Library for rules of use; OA articles are governed by the applicable Creative Commons License

[43] M. H. Chiang, J. A. Dzielawa, M. L. Dietz, M. R. Antonio, *J. Electroanal. Chem.* **2004**, *567*, 77.
[44] M. Ammam, E. B. Easton, *Electrochim. Acta* **2011**, *56*, 2847.
[45] S. Otobe, Y. Kiyota, S. Magira, T. Misawa, K. Fujio, H. Naruke, S. Uchida, T. Ito, *Eur. J. Inorg. Chem.* **2019**, 442.
[46] W. Li, S. Yin, J. Wang, L. Wu, *Chem. Mater.* **2008**, *20*, 514.
[47] X. Lin, W. Li, J. Zhang, H. Sun, Y. Yan, L. Wu, *Langmuir* **2010**, *26*, 13201.
[48] S. Yin, W. Li, J. Wang, L. Wu, *J. Phys. Chem. B* **2008**, *112*, 3983.
[49] X. Tong, V. Thangadurai, *J. Phys. Chem. C* **2015**, *119*, 7621.

Manuscript received: April 7, 2025
Revised manuscript received: May 6, 2025
Version of record online: August 1, 2025

26289725, 2025, 9, Downloaded from https://chemistry-europe.onlinelibrary.wiley.com/doi/10.1002/cmtd.202500046 by Uni Santiago Compostela, Wiley Online Library on [27/11/2025]. See the Terms and Conditions (https://onlinelibrary.wiley.com/terms-and-conditions) on Wiley Online Library for rules of use; OA articles are governed by the applicable Creative Commons License

© 2025 The Author(s). Chemistry - Methods published by Chemistry Europe and Wiley-VCH GmbH